PAPER • **OPEN ACCESS**

Discrete Element Method and Thermodynamics with Internal Variables: Two Complementary Approaches to Link Micro- and Macro-Scale Modelling of Anisotropic Clays

To cite this article: A. G. Pagano *et al* 2025 *IOP Conf. Ser.: Earth Environ. Sci.* **1480** 012047

DISCRETE ELEMENT METHOD AND THERMODYNAMICS WITH INTERNAL VARIABLES: TWO COMPLEMENTARY APPROACHES TO LINK MICRO- AND MACRO-SCALE MODELLING OF ANISOTROPIC CLAYS

A. G. Pagano[1]✉, F. Rollo[2], V. Magnanimo[3], A. Tarantino[4] and A. Amorosi[2]
[1] James Watt School of Engineering, University of Glasgow, UK
[2] Department of Structural and Geotechnical Engineering, Sapienza University of Rome, Italy
[3]Faculty of Engineering Technology, University of Twente, Netherlands
[4]Department Civil and Environmental Engineering, University of Strathclyde, UK
✉ *arianna.pagano@glasgow.ac.uk*

Abstract: This paper presents some preliminary results of a multiscale approach based on the complementary use of the Discrete Element Method (DEM) and the Thermodynamics with Internal Variables (TIV) to model anisotropy of clays. Within this framework, two internal variables, namely porosity and fabric, describe the main features of clay mechanics and keep track of their evolution. In this perspective, DEM results allow to identify an efficient calibration procedure of the microscale model parameters, and to validate the ability of the thermodynamics-based formulation to account for the evolving elastic stiffness anisotropy of clays along different loading paths.

1. Introduction

Anisotropy is defined as the variation of a material property with direction. In soils, anisotropy is believed to arise from specific features evolving upon loading, intrinsically related to the particulate nature of soils. To account for this, continuum constitutive models have included additional 'micro-inspired' internal variables [1, 2], associated with experimental proxies such as the geometrical arrangement/orientation of particles and the size and distribution of the soil porosity. However, the lack of direct experimental evidence capable of quantifying the evolution of these microstructural features poses challenges in the formulation of the evolution law of the internal variables to be used in the constitutive models. A valuable approach to overcome the limitations of physical experiments is to carry out "virtual" experiments using the Discrete Element Method (DEM) [3], where soils are modelled as assemblies of discrete particles, and particle-scale data are readily available to assess the evolution of relevant microstructural features at any point during loading. In this work, an existing DEM framework designed to simulate non-active clays [4] is used to explore the anisotropic character of the elastic properties of clay samples by means of static probing. The corresponding particle-scale mechanisms are then incorporated into a continuum mechanics framework based on Thermodynamics with Internal Variables (TIV) [5]. In the TIV approach, two internal variables are assumed to describe the key features of clay mechanics: porosity, whose evolution reflects into the isotropic hardening of the material, and fabric, responsible for the current directional properties of the soil and their evolution, the latter controlled by a distortional hardening law [6]. In this work, both porosity and fabric (and their evolution) are directly extracted from the DEM simulations and used to calibrate the TIV model parameters, to improve the accuracy and reliability of the predictive ability of the constitutive model.

2. DEM modelling

DEM simulations are conducted in this work on assemblies of rod-shaped particles constrained to move in a plane. Each rod is formed from spherical elementary units bonded together, as proposed in

[4]. The rod-to-rod interaction is modelled using linear-elastic springs between contacting spheres, along with a Coulomb-like friction model. Electro-chemical interactions are simulated using attractive/repulsive long-range forces in the normal direction between spheres not in contact, again by means of linear-elastic springs. In this work, negative charges are assigned to the inner spheres and positive charges to the edges of each rod, simulating clay particles interacting within an acidic pore fluid. Further details on the DEM model parameters and parameter calibration can be found in [4].

An assembly of N_{rod} = 1520 rods is initially generated in a gas-like state (non-contacting rods), resulting in a pressure $p = 0$ and deviator stress $q = 0$. The sample is then isotropically compressed until a fluid-solid transition occurs, *i.e.*, until any further compression results in a pressure increase ($p > 0$, Figure 1, configuration A). Then, the assembly is subjected to two loading paths, as shown in Figure 1: isotropic compression (stress ratio $\eta = 0$, path A-B), or oedometric compression (K_0 loading, path A-C) followed by unloading at constant p (path C-B). To investigate the evolution of rods orientations during loading, a fabric tensor is measured, defined as [7]:

$$\boldsymbol{\beta} = {}^{1}\!/_{N_{rod}} \sum \mathbf{n}^{rod} \otimes \mathbf{n}^{rod} \tag{1}$$

where $\mathbf{n}^{rod}$ is the unit vector oriented with the main axis of each rod. At different stages along the loading paths, the elastic constrained Young moduli of the aggregate are calculated in the axial (v) and transversal (h) directions, by applying an incremental strain and measuring the corresponding stress response within the elastic range: $E_{oed,v} = \Delta\sigma_v/\Delta\varepsilon_v$ and $E_{oed,h} = \Delta\sigma_h/\Delta\varepsilon_h$ [8]. The elastic strain range was identified from the stiffness degradation curve, obtained by obtaining the constrained Young moduli over a large range of strains.

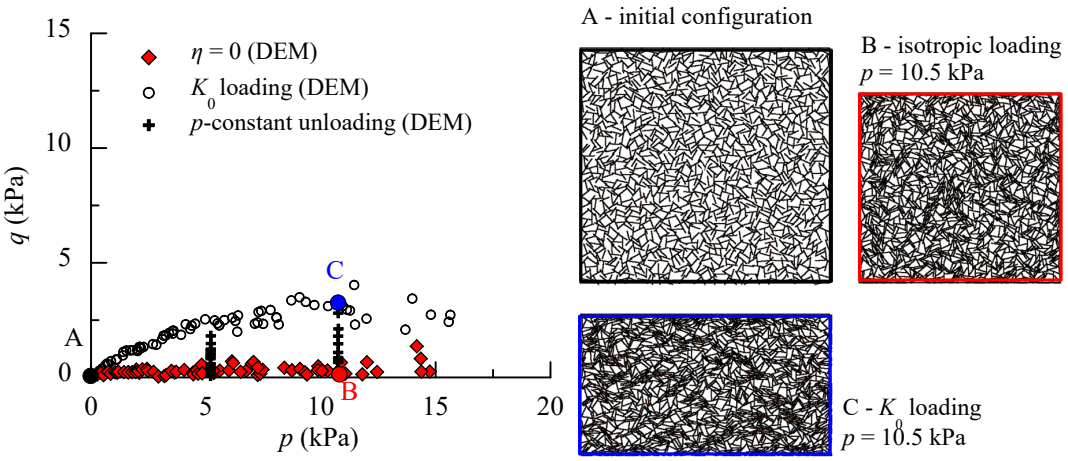

Figure 1. DEM simulations: stress paths and sample configurations at different stages.

3. Thermodynamics-based continuum modelling

According to the TIV, the constitutive behaviour is described by two scalar functions, the free energy and the rate of dissipation potentials, in which the specific volume v and the second order fabric tensor $\boldsymbol{\beta}$ act as internal variables. The additive decomposition of total strains into elastic and plastic is assumed, denoted with the superscript e and p.

The Helmholtz free energy is [6]:

$$\varphi\left(\boldsymbol{\varepsilon}^e, v, \boldsymbol{\beta}\right) = \left(\frac{v}{N}\right)^{\frac{r}{(n-1)\lambda^*}} \frac{p_r}{k(2-n)} k^{\frac{2-n}{1-n}} (1-n)^{\frac{2-n}{1-n}} \left\{ \left[k(1-n) - \frac{2}{3} g \right] \mathrm{tr}^2\left(\boldsymbol{\varepsilon}^e - \omega\beta\boldsymbol{\beta}\boldsymbol{\varepsilon}^e\right) + \right.$$
$$\left. + 2g\,\mathrm{tr}\left[\left(\boldsymbol{\varepsilon}^e - \omega\beta\boldsymbol{\beta}\boldsymbol{\varepsilon}^e\right)^2 \right] \right\}^{\frac{2-n}{2-2n}} \tag{2}$$

where p_r is a reference pressure, N is the specific volume at p_r; n, k and g are the parameters of the hyperelastic potential to account for the nonlinear dependence of the elastic stiffness on the current stress/elastic strain, while r and ω control the dependence of the elastic stiffness on v and the magnitude of anisotropy, respectively. β represents the invariant of $\boldsymbol{\beta}$ (*i.e.*, its triaxial counterpart).

For the rate of dissipation, the following expression is adopted [6]:

$$\dot{d}\left(v, \boldsymbol{\beta}, \dot{\boldsymbol{\varepsilon}}^p, \dot{v}, \dot{\boldsymbol{\beta}}\right) = \frac{p_r}{2}\left(\frac{v}{N}\right)^{-\frac{1}{\lambda^*}} \left(\dot{\bar{d}} + \dot{\varepsilon}_v^p + \boldsymbol{\beta} : \dot{\boldsymbol{\varepsilon}}'^p\right) + I_{\mathrm{K}}\left(\frac{\dot{v}}{v} + \dot{\varepsilon}_v^p\right) + I_{\mathrm{L}}\left[\dot{\boldsymbol{\beta}} - c\left(\boldsymbol{\beta}_b - \boldsymbol{\beta}\right)\dot{\bar{d}}\right] \tag{3}$$

with

$$\dot{\bar{d}} = \sqrt{\left(\dot{\varepsilon}_v^p + \boldsymbol{\beta} : \dot{\boldsymbol{\varepsilon}}'^p\right)^2 + \frac{2}{3}\left(M^2 - \beta^2\right)\dot{\boldsymbol{\varepsilon}}'^p : \dot{\boldsymbol{\varepsilon}}'^p}\,, \tag{4}$$

in which the prime denotes the deviatoric part of the strain tensor, M is the stress ratio at critical state, λ^* is the parameter governing the isotropic hardening law, $\boldsymbol{\beta}_b$ is the bounding value of $\boldsymbol{\beta}$ according to the exponential law proposed by [9] and c controls the pace of evolution of $\boldsymbol{\beta}$. The last terms of Eq. (3) are two indicator functions acting as constraints for the rate evolution of v and $\boldsymbol{\beta}$.

The model parameters are shown in Table 1. The calibration procedure is performed with reference to the DEM results. Specifically, the elastic parameters are selected to reproduce the elastic stiffness under isotropic loading, and the exponent r is deduced from the elastic probing along the unloading paths at constant p. The parameter λ^* is deduced from the compressibility curves (Figure 2a, b), while c, s, z and ω are chosen to reproduce the fabric evolution, all obtained from the DEM simulations (Figure 2c).

p_r (kPa)	g	k	n	R	N	λ^*	M	c	s	z	ω
100	48	64	0.17	0.63	1.3	0.25	1.1	1.2	14	5.4	25

Table 1. Model parameters

Figure 2 (d) shows the comparison between the constrained moduli obtained from DEM simulations, and the TIV model predictions. The DEM simulation results show that: a) isotropically-compressed samples, characterised by an isotropic fabric (random particle orientations) at any state along the η = 0 path, exhibit an isotropic behaviour, with similar values of vertical and horizontal elastic moduli for each given state of stress and porosity; b) samples compressed along K_0-loading path are characterised by a progressively anisotropic fabric upon loading, with samples becoming stiffer along the horizontal direction, compared to the vertical direction. Once calibrated on the fabric evolution, the TIV model is able to successfully back-predict elastic stiffness anisotropy and its evolution during K_0-loading.

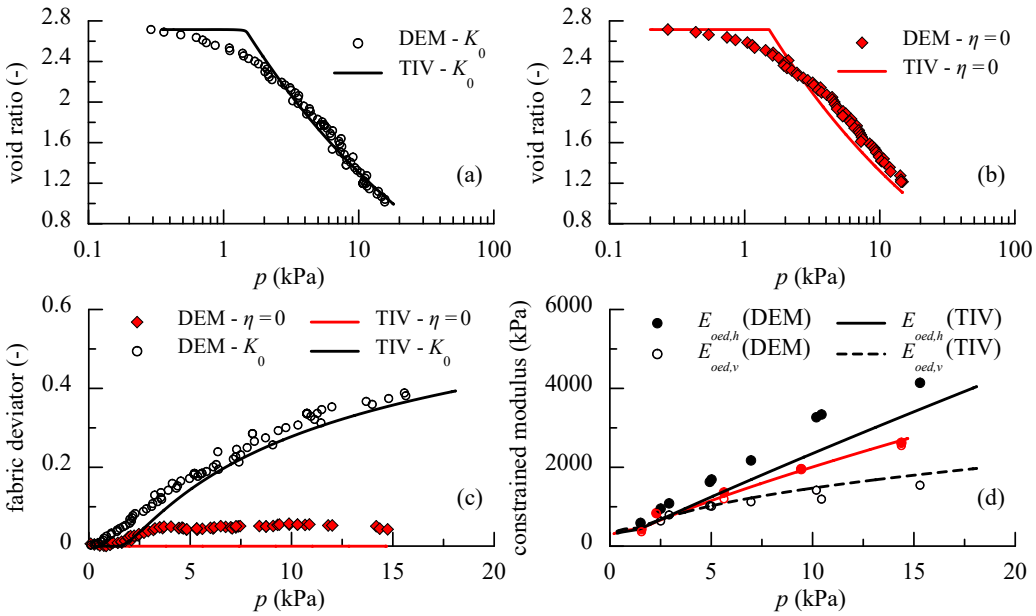

Figure 2. Results of DEM and TIV simulations for K_0- and isotropic loading: compressibility curves (a, b), fabric deviator (c) and constrained moduli (d).

4. Acknowledgements

A. Amorosi and F. Rollo acknowledge the RETURN Extended Partnership and received funding from the European Union Next-GenerationEU (National Recovery and Resilience Plan – NRRP, Mission 4, Component 2, Investment 1.3 – D.D. 1243 2/8/2022, PE0000005).

References:

[1] Fu, P., & Dafalias, Y. F. (2015). Relationship between void-and contact normal-based fabric tensors for 2D idealized granular materials. *Int. Journal of Solids and Structures*, *63*, 68-81.

[2] Amorosi, A., Rollo, F., & Dafalias, Y. F. (2021). Relating elastic and plastic fabric anisotropy of clays. *Géotechnique*, *71*(7), 583-593.

[3] Cundall, P. A. and Strack, O. D. L. (1979). A discrete numerical model for granular assemblies. *Géotechnique*, *29* (1), 47-65.

[4] Pagano, A.G., Magnanimo, V., Weinhart, T., and Tarantino, A. (2020). Exploring the micromechanics of non-active clays by way of virtual DEM experiments. *Géotechnique*, *70*(4), 303-316.

[5] Maugin, G.A., Muschik W. (1994). Thermodynamics with internal variables. I. General Concepts, II. Applications. *Journal of Non-Equilibrium Thermodynamics*, *19*, 217-249, 250-289.

[6] Amorosi, A., Rollo F., Di Santo G. (2023). A micro-inspired perspective on the constitutive modelling of clays. *Rivista Italiana di Geotecnica*, 4, 3-22.

[7] Oda, M., Nemat-Nasser, S. & Konishi, J. (1985). Stress-induced anisotropy in granular masses. *Soils and Foundations, 25*(3), 85-87.

[8] La Ragione, L. and Magnanimo, V. (2012). Evolution of the effective moduli of an anisotropic, dense, granular material. *Granular Matter 14*(6), 749-757.

[9] Dafalias, Y. F., & Taiebat, M. (2013). Anatomy of rotational hardening in clay plasticity. *Géotechnique*, *63*(16), 1406-1418.